Monthly Notices of the ROYAL ASTRONOMICAL SOCIETY

MNRAS **473,** L74–L78 (2018) doi:10.1093/mnrasl/slx165
Advance Access publication 2017 October 9

Evidence of Compton cooling during an X-ray flare supports a neutron star nature of the compact object in 4U1700−37

M. Martinez-Chicharro,[1⋆] J. M. Torrejón,[1⋆] L. Oskinova,[2⋆] F. Fürst,[3] K. Postnov,[4] J. J. Rodes-Roca,[1] R. Hainich[2] and A. Bodaghee[5]

[1]*Instituto Universitario de Física Aplicada a las Ciencias y las Tecnlogías, Unversidad de Alicante, E-03690 Alicante, Spain*
[2]*Institute for Physics and Astronomy, Universität Potsdam, D-14476 Potsdam, Germany*
[3]*European Space Astronomy Centre (ESAC), Science Operations Departement, E-28692 Villanueva de la Cañada, Madrid, Spain*
[4]*Sternberg Astronomical Institute, Moscow M.V. Lomonosov State University, E-119234 Moscow, Russia*
[5]*Department of Chemistry, Physics and Astronomy, Georgia College, 221 N. Wilkinson St, Milledgeville, GA 31061, USA*

Accepted 2017 October 4. Received 2017 September 13; in original form 2017 July 7

ABSTRACT

Based on new *Chandra* X-ray telescope data, we present empirical evidence of plasma Compton cooling during a flare in the non-pulsating massive X-ray binary 4U1700−37. This behaviour might be explained by quasi-spherical accretion on to a slowly rotating magnetized neutron star (NS). In quiescence, the NS in 4U1700−37 is surrounded by a hot radiatively cooling shell. Its presence is supported by the detection of mHz quasi-periodic oscillations likely produced by its convection cells. The high plasma temperature and the relatively low X-ray luminosity observed during the quiescence, point to a small emitting area ∼1 km, compatible with a hotspot on an NS surface. The sudden transition from a radiative to a significantly more efficient Compton cooling regime triggers an episode of enhanced accretion resulting in a flare. During the flare, the plasma temperature drops quickly. The predicted luminosity for such transitions, $\sim 3 \times 10^{35}$ erg s^{-1}, is very close to the luminosity of 4U1700−37 during quiescence. The transition may be caused by the accretion of a clump in the stellar wind of the donor star. Thus, a magnetized NS nature of the compact object is strongly favoured.

Key words: stars: individual: 4U1700−37, V*V884 Sco – X-rays: binaries.

1 INTRODUCTION

High-mass X-ray binaries (HMXBs) are fundamental laboratories where the structure of the stellar wind in massive stars as well as the physics of accretion on to compact objects can be studied in detail (Martínez-Núñez et al. 2017, for a recent review). One of the best studied HMXBs in the Galaxy, 4U1700−37, consists of a O6Iafcp donor star (V*V884 Sco; Sota et al. 2014) and a compact object on the 3.41 d orbit at an average orbital distance of $a \approx 1.6R^*$.

Despite the vast amount of multiwavelength observational data accrued so far, the nature of the compact object in 4U1700−37, remains a mystery. No coherent pulsations have ever been found in X-rays or any other wavelengths. The mass determinations of the compact object give $2.44 \pm 0.27\,M_\odot$ (Clark et al. 2002), quite high for a neutron star[1] (NS), but too low compared with the smallest black hole (BH) found so far. Indirect evidence supporting the presence of an NS has been provided based on the X-ray spectra (Seifina, Titarchuk & Shaposhnikov 2016) or the X-ray colour–colour behaviour (Vrtilek & Boroson 2013). A BH, in turn, has been favoured based on timing properties (Dolan 2011).

The donor star in 4U1700−37 , V*V884 Sco, is one of the most massive stars ($M^* = 58 \pm 11\,M_\odot$) known in the Galaxy and the most massive donor known in any Galactic HMXB. The inner parts of OB-star winds ($a < 2R^*$) are inhomogeneous and clumped (Torrejón et al. 2015) but their properties are not well known. In the past, several studies have used the compact object in 4U1700−37 to probe *in situ* the donor star wind. Haberl, White & Kallman (1989), using *EXOSAT*, studied the radial wind density stratification, via photoelectric absorption. van der Meer et al. (2005) performed a study of the emission lines excited in the stellar wind by the powerful X-ray source, using *XMM–Newton*. Hints of highly ionized iron were detected but could not be completely disentangled from the nearly neutral Fe Kα line at the *EPIC-CCD* resolution. The *XMM–Newton* light curves showed an *off state*, when the X-ray count rate dropped to zero for a short time. van der Meer et al. (2005) attributed this off state to the gap between two successive clumps propagating in the stellar wind.

In this Letter, we present a 14 ks *Chandra* observation of 4U1700−37 during which the source flared. This enables us to investigate the changes in spectral properties at different luminosities.

This Letter is structured as follows: in Section 2, we present the observational details. In Sections 3 and 4, we analyse the light curve and time-resolved spectra of the source, providing the best-fitting

⋆ E-mail: maria.martinez@ua.es (MM-C); jmt@ua.es (JMT); lida@astro.physik.uni-postdam.de (LO)

[1] Although still below the Tolman–Oppenheimer–Volkoff limit of ∼3 $M_\odot$.

Table 1. Observations journal.

ObsID	Date	t_{exp}	ϕ_{orb}
17630	2015-02-22 03:11:16	14.27	0.13[a]

Note. [a]Mid eclipse time $T_0 = 49\,149.412 \pm 0.006$ MJD, orbital period $P = 3.411\,660 \pm 0.000\,004$ d (Islam & Paul 2016).

parameters for the continuum and the Fe emission lines. Finally, in Sections 5 and 6, we discuss these parameters in the framework of the theory and present the conclusions.

2 OBSERVATIONS

The DDT observations of 4U1700−37 were performed by *Chandra* on 2015 Feb 22 simultaneously with the *Hubble Space Telescope* (*HST* , P.I. L. Oskinova).[2] The High Energy Transmission Gratings spectrometer onboard of *Chandra* (HETG; Canizares et al. 2005) acquired data during a total of 14.27 ks. The HETG provides spectra with two sets of gratings, the High Energy Grating (HEG) which offers a resolution of 0.011 Å in the bandpass of about 1.5–16 Å, and the Medium Energy Grating (MEG) which offers a resolution of 0.021 Å in the bandpass of about 1.8–31 Å. The spectra were reduced using standard procedures with the CIAO software (v 4.4) and the response files were generated (`arf` and `rmf`). First dispersion orders ($m = \pm 1$) were extracted and analysed simultaneously. The peak source flux both at HEG and MEG gratings is 4.4 s^{-1}, which is much lower than the level at which pileup starts to be important.[3] The spectral analysis was performed with the Interactive Spectral Interpretation System (ISIS) v 1.6.1–24 (Houck & Denicola 2000). The details of the observation can be found in Table 1.

3 LIGHT CURVES AND TIMING

Fig. 1 shows the extracted light curves in the hard 1.5–4 Å (H) and soft 4–15 Å (S) bands. Both light curves are strongly variable as typical in wind accreting HMXBs. Two episodes are remarkable. The most obvious one lasts from ∼7600 to 13 000 s when the source undergoes a flare after which it returns to the quiescence brightness levels. The hardness ratio, HR=H−S/H+S, does not show any noticeable change, even during the flare. The second episode is the period of very low flux, between 7200 and 7350 s, preceding the flare. During the low-flux period, the count rate in the soft band is consistent with zero counts. Similar *off-states* are often observed in systems containing magnetized NS (eg. Vela X-1; Kreykenbohm et al. 2008). To our knowledge, the off-states have not been observed in HMXBs that contain a BH.

In the right-hand panel of Fig. 1, we show the standard Lomb–Scargle periodogram of *Chandra* HETG 1.5–10 Å light curve, binned to 5 s, separately for the quiescence and flare. In agreement with previous observations, we do not see any signatures of coherent pulsations. However, the periodogram clearly shows several mHz quasi-periodic oscillations (QPOs) more noticeable during the flare. The false alarm probability of the 0.63 ± 0.05 mHz peak is lower than 1 per cent. Such QPOs at mHz frequencies have already been reported for 4U1700−37 on the basis of *Chandra* (Boroson et al. 2003) and *RXTE* observations (Dolan 2011).

[2] The *HST* UV observations will be reported in the follow-up publication, Hainich et al. (in preparation).

[3] See *The Chandra ABC Guide to Pileup*, v.2.2, http://cxc.harvard.edu/ciao/download/doc/pileup-abc.pdf

4 SPECTRA

4.1 Continuum modelling

In order to shed light on the mechanism that triggered the flare, we want to trace plasma changes by performing time resolved spectroscopy during the time intervals t = [0–7600, 13 000–14 200] s (quiescence) and t = [7600–13 000] s (flare). We successfully fit the continuum with the bulk motion Comptonization model (BMC) (Titarchuk, Mastichiadis & Kylafis 1997) Fig. 2. BMC is a general model for Comptonization of soft photons which uses the Green's (spread) functions for the treatment of upscattering and which attains the form of a broken power law. This formalism is valid for any kind of Comptonization (bulk Comptonization in first order (v/c), thermal Comptonization in second order $(v/c)^2$) and remains valid up to photon energies comparable to the mean plasma energy ($m_e c^2 \sim 511$keV in the case of bulk motion). In the case of a BH, the soft component originates in the innermost part of the accretion disc where the gravitational energy of matter is released due to viscous dissipation and geometric compression. In the case of an NS, the soft component is likely produced by a hotspot on the NS surface. Either the disc or the surface (or both) emits a soft blackbody-like spectrum with a characteristic colour temperature kT_{col}. The Comptonizing region (a cloud or a boundary layer) must cover effectively this zone (i.e. the innermost region of the disc or the spot over the surface) in order to be well exposed to a high fraction of the seed photons. Parameter f describes the ratio of the number of photons multiply scattered in the converging inflow to the number of photons in the thermal component. During fitting procedure we have fixed it at 10 ($\gg$1) meaning that the Compton cloud efficiently covers the soft photons source.[4]

One of the three free parameters of the BMC model is a power-law spectral index α describing the Comptonization efficiency. When α is smaller, the spectrum is harder due to enhanced efficiency (for details see Sunyaev & Titarchuk 1980). On the contrary, larger α describes softer spectra. A value close to unity indicates that the source is undergoing a phase transition from the low-hard to a high-soft state. The transitions can be caused by a number of mechanisms, e.g. the redistribution of mass accretion rates between Keplerian disc and sub-Keplerian components in a disc or by an increase of the optical depth τ_0 for gravitational energy release at the shock (BH case) or at the surface (NS case).

The emitted X-ray continuum described above must be modified at low energies by photoelectric absorption ABS(E) in order to account for the local and interstellar absorption effects. The observed continuum is thus $F(E)$ =ABS(E)× BMC(E) where the absorber is described by

$$\mathrm{Abs}(E) = \left(\epsilon \times \mathrm{e}^{-\sigma(E)N_{\mathrm{H},1}} + (1-\epsilon) \times \mathrm{e}^{-\sigma(E)N_{\mathrm{H},2}}\right) \quad (1)$$

Here, ϵ is the *covering fraction* which acts as a proxy for the massive star wind clumping. The photoelectric absorption has been modelled using `tbnew` which contains the most up to date cross-sections for X-ray absorption.[5] The best-fitting parameters are presented in Table 2.

During quiescence, the column density $N_{H,2} = N_H^{ISM} = 0.30^{+0.28}_{-0.23} \times 10^{22}$ cm^{-2} is compatible with the interstellar medium (ISM) absorption towards V*V884 Sco, deduced from the optical extinction, $E(B-V) = 0.54 \pm 0.02$ (Clark et al. 2002) and using the

[4] Given the limited energy range covered by *Chandra*, the model is not sensitive to the exact value of f.

[5] http://pulsar.sternwarte.uni-erlangen.de/wilms/research/tbabs/index.html

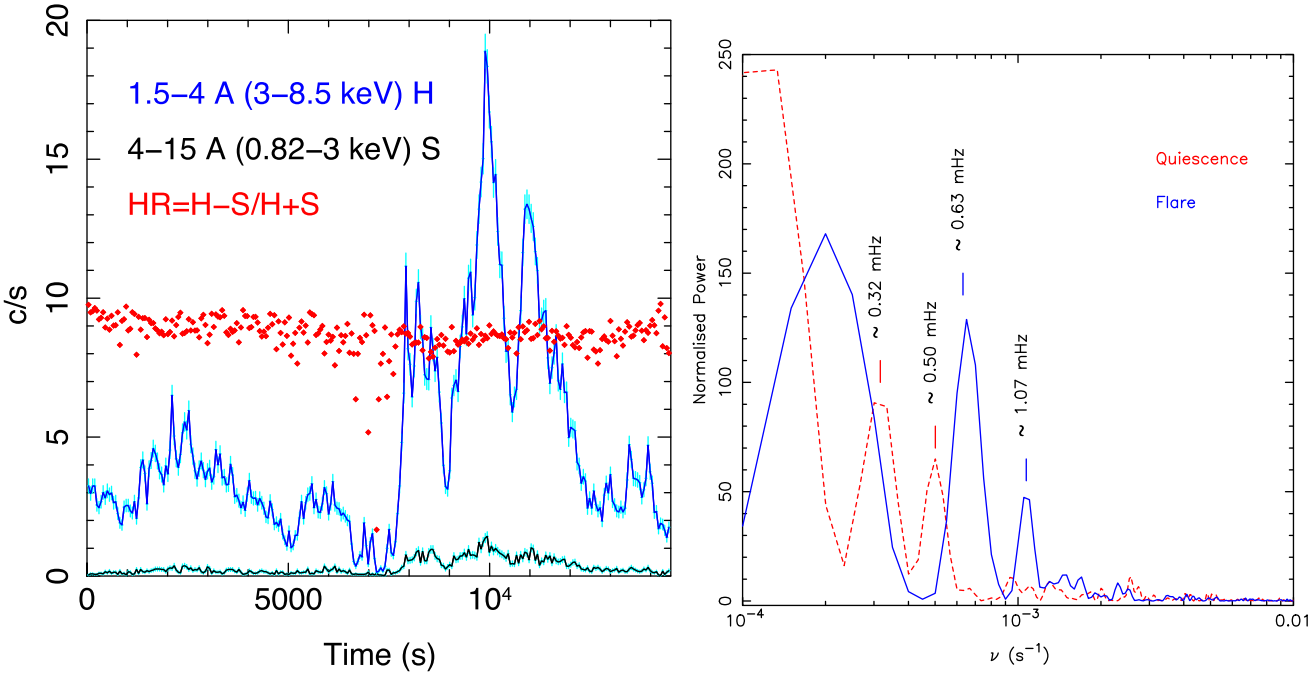

Figure 1. *Chandra* HETG light curve, in the 1.2–15 Å wavelength range, grouped in 10 s bins. The HR seems to be constant even during the flare. Right-hand panel: Lomb–Scargle periodogram of the *Chandra* HETG light curve binned to 5 s for quiescence and flare. No coherent period is found but a number of ∼ mHz QPOs are detected, most prominently during the flare.

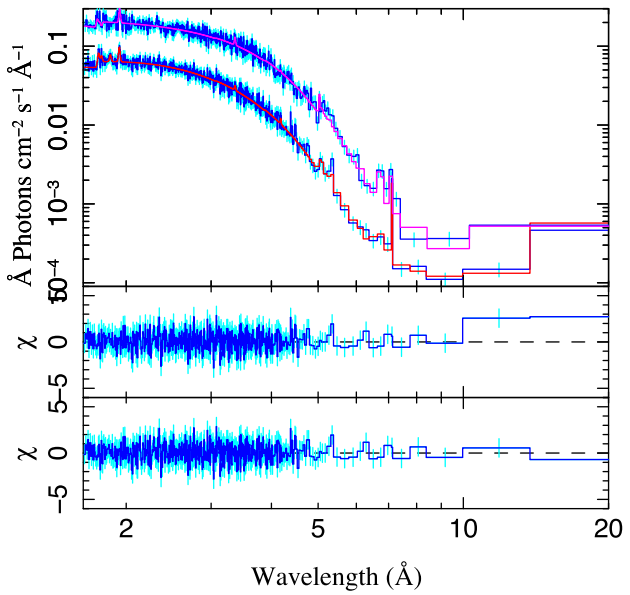

Figure 2. The *Chandra* HETG spectra during quiescence and flare grouped in 5σ bins. Residuals are shown for the BMC model (mid panel) during quiescence (residuals during flare are similar). The soft excess seen at long wavelengths, found in the spectra of many HMXBs (Hickox, Narayan & Kallman 2004), can be described by the addition of a blackbody with $N_{\rm H,\,3}$ (10^{22} cm^{-2}) $= 0.3 \pm 0.1$ and $kT_{\rm bb} = 0.095^{+0.007}_{-0.011}$ keV (bottom panel). This component, however, is marginal and its addition here does not improve the fit.

relationship $N_{\rm H} = 6.12 \times 10^{21} E(B-V)$ (Gudennavar et al. 2012). On the other hand, $N_{\rm H,\,1}$ is much larger during the flare, consistent with the thick stellar wind expected in a O6.5 supergiant star.

The spectral power-law index α goes from ∼1.2 during quiescence to ∼0.19 during the flare showing that the Comptonization is more efficient when the luminosity (presumably the mass accretion rate) increases. At the same time, the soft photon source temperature $kT_{\rm col}$ decreases from 1.43 keV (∼16 MK) to 0.58 keV (7 MK) during the flare when the Comptonization (hence the Compton cooling) is more efficient. Thus, we observe plasma that cooled down by about 9 million degrees on the time-scale of an hour.

Table 2. Model BMC continuum parameters.

Parameter	Quiescence	Flare
	BMC	
$N_{\rm H,\,1}$ (10^{22} cm^{-2})	$18.9^{+0.2}_{-0.2}$	$19.36^{+0.19}_{-0.19}$
ϵ	$0.995^{+0.001}_{-0.001}$	$0.994^{+0.001}_{-0.001}$
$N_{\rm H,\,2}$ (10^{22} cm^{-2})	$0.30^{+0.30}_{-0.20}$	$2.53^{+0.36}_{-0.30}$
Norm	$0.0142^{+0.0001}_{-0.0001}$	$0.0627^{+0.0006}_{-0.0006}$
$kT_{\rm col}$ (keV)	$1.43^{+0.01}_{-0.01}$	$0.58^{+0.01}_{-0.01}$
α	$1.25^{+0.04}_{-0.03}$	$0.186^{+0.003}_{-0.003}$
f	10 (fixed)	10 (fixed)
Flux[a]	$8.00^{+0.05}_{-0.05}$	$45.00^{+0.27}_{-0.27}$
$\chi^2_{\rm r}$(d.o.f.)	0.96(443)	0.98(467)

Note. [a]Unabsorbed 1.5–20 Å flux, $\times\ 10^{-10}$ erg s^{-1} cm^{-2}.

4.2 Fe lines

The plasma cooling during the flare due to enhanced Compton efficiency is strongly supported by the analysis of the highly ionized iron lines. Fig. 3 shows the Fe Kα line region during quiescence and flare. The quiescence spectra (left-hand panel) show lines from the low ionized Fe (Kα and Kβ fluorescence, along with the Fe K edge at 1.7 keV) as well as from highly ionized states (Fe XXV He-like and Fe XXVI H-like Lyα). These transitions arise in the circumsource material illuminated by the powerful source of X-rays from the

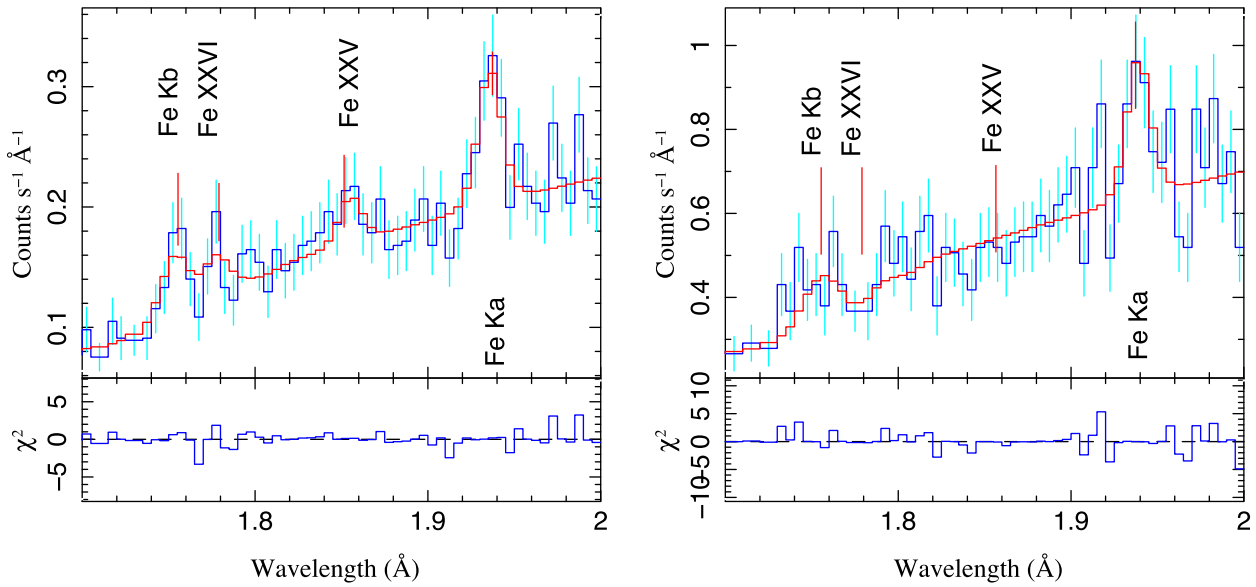

Figure 3. *Chandra* HETG spectra and the best-fitting model, in the 1.6–2.1 Å range, during quiescence (left) and flare (right), respectively. The lower panels show the quality of fit.

Table 3. Fe lines parameters. Numbers without errors have been fixed at the quoted values.

	Quiescence				Flare			
Ion	λ (Å)	Flux $\times 10^{-6}$ (ph s^{-1} cm^{-2})	σ (Å)	EW (mÅ)	λ (Å)	Flux $\times 10^{-6}$ (ph s^{-1} cm^{-2})	σ (Å)	EW (mÅ)
Fe Kβ	$1.753^{+0.003}_{-0.004}$	190^{+180}_{-90}	0.005	21^{+6}_{-6}	$1.756^{+0.052}_{-0.052}$	251^{+400}_{-150}	0.005	8^{+1}_{-7}
Fe XXVI Lyα	$1.777^{+0.002}_{-0.006}$	125^{+80}_{-125}	0.005	7^{+24}_{-4}	$1.777^{+0.002}_{-0.011}$	-240^{+290}_{-430}	0.005	-8^{+1}_{-13}
Fe XXV	$1.855^{+0.004}_{-0.000}$	170^{+100}_{-50}	0.005	18^{+18}_{-1}	$1.855^{+0.004}_{-0.004}$	$0.00^{+192}_{-0.01}$	0.005	$0.0^{+0.4}_{-0.1}$
Fe Kα	$1.935^{+0.003}_{-0.003}$	330^{+120}_{-90}	0.005	33^{+11}_{-8}	$1.939^{+0.004}_{-0.003}$	970^{+30}_{-380}	0.005	$31.3^{+0.7}_{-12.2}$

accretion on to the compact object. In order to measure line fluxes, we fitted them as Gaussians. Table 3 lists corresponding best-fitting parameters.

During the flare, the Kα fluorescence line from nearly neutral Fe remain largely unaffected. The line flux increases in response to the increased illumination (higher X-ray continuum) but the equivalent width (EW) stays constant (see Table 3). In contrast, the highly ionized species (He-like Fe XXV and H-like Fe XXVI Lyα), disappear. These lines are produced in very high temperature plasma. During the episode of enhanced cooling, the Fe ionization drops and these lines should become less prominent. This is indeed confirmed by observations. On the other hand, the transition of H like Fe XXVI Ly α seems to appear in absorption during the flare, hinting to the presence of a warm absorber, although the large associated errors prevent a firm conclusion. At any rate, the highly ionized Fe lines decrease significantly (or vanish) during the flare.

5 DISCUSSION

The phenomenology presented above can be readily explained as an episode of Compton plasma cooling during a flare. This behaviour is predicted in accreting NS systems with moderate X-ray luminosities, undergoing quasi-spherical subsonic accretion (Shakura et al. 2012).

At a distance of $d \simeq 2$ kpc (Ankay et al. 2001; Megier et al. 2009), the (un absorbed) luminosity of 4U1700−37 is $L_X \approx 4 \times 10^{35}$ erg s^{-1} during quiescence. At such luminosities, direct (Bondi) wind accretion is hampered by the need of the plasma to cool. If $t_{cool} \gg t_{freefall}$, the matter undergoes subsonic settling accretion and a quasi-spherical shell appears around the NS between the magnetospheric radius and the Bondi radius. The presence of a convective shell is supported by the presence of mHz QPOs in the light curve. These QPOs might reflect the convective motions inside the shell.

On the other hand, the luminosity of 4U1700−37 in quiescence is very close to the threshold predicted for a phase transition from radiative to Compton cooling, $\sim 3 \times 10^{35}$ erg s^{-1} (Shakura, Postnov & Hjalmarsdotter 2013). Hence, 4U1700−37 is very prone to such transitions which may easily be caused by a local perturbation in the accretion flow. Following the transition, the enhanced efficiency of the Compton cooling further increases the ability of matter to enter the magnetosphere and accrete. This runaway process leads to a flare. During the observed flare, the luminosity reached $L_X \approx 2 \times 10^{36}$ erg s^{-1}, still too low for the direct Bondi accretion regime.

In our observation, the flare is preceded by an off state (see Fig. 1). As a possible explanation for these observational facts, one may consider a clumped stellar wind, where the medium between clumps is strongly rarefied (Oskinova, Feldmeier & Kretschmar 2012). In this case, a perturbation caused by the ingestion of a wind clump

(flare) would be preceded by a short period of time when the wind in the vicinity of the NS is void (off state).

At the quasi-spherical settling accretion stage, the NS equilibrium spin period can be very long, about 1000 s for the canonical NS magnetic field 10^{12} G and typical stellar wind velocities of about 1000 km s^{-1} (Shakura et al. 2012). The spin period is almost directly proportional to the NS magnetic field, and for a highly magnetized NS can be a few ten thousand seconds or even longer (Sidoli et al. 2017, 36.2 ks in AX J1910.7+091). This may explain the non-detection of coherent pulsations.

Despite the lack of pulse detection, other pieces of evidence support the presence of a magnetized NS. The temperature of the soft photons is rather high during quiescence. To reconcile the high colour temperature of the soft emitting region $T_{\rm col} \sim 1.4$ keV with the low intrinsic luminosity($L_{\rm X} \sim 10^{35}$ erg s^{-1}) a small emission area must be invoked. Assuming that the source is radiating as a blackbody of area $4\pi R_W^2$, the radius of the emitting area would be $R_W = 0.3\sqrt{L_{34}}(kT_{\rm col}/1{\rm kev})^{-2} \simeq 0.9$ km, which is only compatible with a hotspot over the NS surface. On the other hand, during the flare this radius turns out to be much larger, of the order of 12 km, comparable in size to the entire NS.

6 CONCLUSIONS

We present empirical evidence of plasma Compton cooling during a flare in 4U1700−37. This is supported by the analysis of the X-ray continuum as well as the disappearance of the highly ionized Fe lines. This behaviour can be explained by the sudden accretion of the hot shell that forms around the NS when a transition from a radiative cooling regime to a much more efficient Compton cooling occurs. The predicted luminosity for such transitions, namely $\sim 3 \times 10^{35}$ erg s^{-1} (Shakura et al. 2013) is very close to where 4U1700−37 stays during quiescence. The presence of such hot shell is further supported by the detection of mHz QPOs produced by convection cells in the shell. To reconcile the high plasma temperature with the low L_X, a small emitting area $R_W \sim 1$ km, must be invoked, only compatible with a hotspot on an NS surface. Therefore, a magnetized NS is strongly favoured by the available data. The lack of coherent pulsations may indicate a very long spin period of a strongly magnetized NS with $B > 10^{13}$ G.

ACKNOWLEDGEMENTS

This research has been supported by the grant ESP2014-53672-C3-3P. AB acknowledges support from STScI award 44A-1096046. JJRR acknowledges support from MECD fellowship PRX17/00114. This research has made use of the ISIS functions provided by ECAP/Remeis observatory and MIT. We thank *Chandra* director for the approval of the Director's Discretionary Time observation and the anonymous referee whose comments improved the content of the Letter.

REFERENCES

Ankay A., Kaper L., de Bruijne J. H. J., Dewi J., Hoogerwerf R., Savonije G. J., 2001, A&A, 370, 170
Boroson B., Vrtilek S. D., Kallman T., Corcoran M., 2003, ApJ, 592, 516
Canizares C. R. et al., 2005, PASP, 117, 1144
Clark J. S., Goodwin S. P., Crowther P. A., Kaper L., Fairbairn M., Langer N., Brocksopp C., 2002, A&A, 392, 909
Dolan J. F., 2011, preprint (arXiv:1107.1537)
Gudennavar S. B., Bubbly S. G., Preethi K., Murthy J., 2012, ApJS, 199, 8
Haberl F., White N. E., Kallman T. R., 1989, ApJ, 343, 409
Hickox R. C., Narayan R., Kallman T. R., 2004, ApJ, 614, 881
Houck J. C., Denicola L. A., 2000, in Manset N., Veillet C., Crabtree D., eds, ASP Conf. Ser. Vol. 216, Astronomical Data Analysis Software and Systems IX. Astron. Soc. Pac., San Francisco, p. 591
Islam N., Paul B., 2016, MNRAS, 461, 816
Kreykenbohm I. et al., 2008, A&A, 492, 511
Martínez-Núñez S. et al., 2017, Space Sci. Rev., 212, 59
Megier A., Strobel A., Galazutdinov G. A., Krełowski J., 2009, A&A, 507, 833
Oskinova L. M., Feldmeier A., Kretschmar P., 2012, MNRAS, 421, 2820
Seifina E., Titarchuk L., Shaposhnikov N., 2016, ApJ, 821, 23
Shakura N., Postnov K., Kochetkova A., Hjalmarsdotter L., 2012, MNRAS, 420, 216
Shakura N., Postnov K., Hjalmarsdotter L., 2013, MNRAS, 428, 670
Sidoli L., Israel G. L., Esposito P., Rodríguez Castillo G. A., Postnov K., 2017, MNRAS, 469, 3056
Sota A., Maíz Apellániz J., Morrell N. I., Barbá R. H., Walborn N. R., Gamen R. C., Arias J. I., Alfaro E. J., 2014, ApJS, 211, 10
Sunyaev R. A., Titarchuk L. G., 1980, A&A, 86, 121
Titarchuk L., Mastichiadis A., Kylafis N. D., 1997, ApJ, 487, 834
Torrejón J. M., Schulz N. S., Nowak M. A., Oskinova L., Rodes-Roca J. J., Shenar T., Wilms J., 2015, ApJ, 810, 102
van der Meer A., Kaper L., di Salvo T., Méndez M., van der Klis M., Barr P., Trams N. R., 2005, A&A, 432, 999
Vrtilek S. D., Boroson B. S., 2013, MNRAS, 428, 3693

This paper has been typeset from a TEX/LATEX file prepared by the author.